Mirosław JAKUBOWSKI ⓘ

Optimization of the cooling system in a prototype VCR engine using CFD analysis

ARTICLE INFO

The cooling system of an internal combustion engine affects various key parameters, including ignition delay, fuel evaporation, and the compression-expansion process. The geometry of its components impacts both cooling efficiency and the energy demand of the coolant pump. This paper presents CFD simulation results of coolant flow through selected elements of a modified cooling system in a prototype engine. Due to design changes in the power unit, the original coolant outlet manifold required redesign. Three manifold variants were analyzed under two coolant types and two back pressure levels. Flow patterns were evaluated using streamlines and velocity distributions in selected cross-sections. The applied manifold modification significantly increased coolant velocity. In the analyzed cases, the local resistance coefficient rose to values as high as 9. For version mod2, the risk of turbulence was higher with a water-glycol mixture than with water. For version mod1, turbulence sensitivity to coolant type was negligible.

1. Introduction

One of the fundamental conditions for the proper operation of internal combustion engines is maintaining adequate cooling intensity. Parameters of the cooling process, such as coolant flow rate, significantly influence heat exchange between the coolant and the heated walls of the cylinders and cylinder head. Additionally, cooling intensity affects pressure changes during the compression and expansion strokes, as well as the fuel evaporation process and ignition delay time in compression ignition engines. The thermal state of the engine also plays a crucial role in determining the quality of the air-fuel mixture.

In traction-type internal combustion engines, liquid cooling with forced circulation is almost universally applied. Approximately 30% of the heat generated during combustion is transferred to the coolant [23], representing a substantial thermal load. Ensuring proper coolant flow – achieved, for example, through the optimized geometry of cooling system components – is essential. For this purpose, commercial Computational Fluid Dynamics (CFD) software is commonly utilized [10].

Numerical analysis of coolant flow in internal combustion engine cooling systems must account for turbulence. The k–ε turbulence model is widely used due to its robustness and suitability for this application [2, 4, 13, 16]. CFD simulations typically consider both fluid dynamics and thermal interactions between the coolant and the walls of the flow passages [3, 17]. Phenomena such as cavitation [7, 12] and other flow disturbances are also relevant in such analyses. Since velocity distribution in coolant channels determines heat transfer efficiency, it is a critical aspect of CFD-based investigations.

The effect of the study [5] demonstrates that modifying the water jacket can reduce the volume of stagnant coolant by up to 75% and increase flow velocity by as much as 50%, compared to the original design. CFD simulations can also predict flow and thermal non-uniformities and identify zones of low velocity [19, 21, 22, 24]. These tools are increasingly applied in the thermal management of electric vehicle systems as well [6, 11].

Numerical flow analysis is also employed in the development and optimization of air-cooled engine systems. Simulations enable assessment of fin design with varying geometrical and material properties, and facilitate the estimation of thermal stresses [14, 15, 18, 20]. As shown in [20], simulation results exhibited good correlation with data obtained from wind tunnel experiments.

Cooling of internal combustion engines also involves heat dissipation through oil. Analyzing its flow using CFD offers benefits, such as reducing prototyping time, particularly in conditions of variable flow channel dynamics. This occurs, for instance, in connecting rods, where oil flows to cool the piston [8].

Designing modern internal combustion engines involves a wide array of requirements, including those pertaining to thermal management. The application of CFD tools facilitates rapid evaluation of various design configurations, enabling selection of appropriate geometries for manifolds, channels, hoses, and other components.

The subject of this study is a prototype diesel engine with a variable compression ratio, developed based on a commercially available four-stroke, inline four-cylinder engine. A distinguishing feature of the design is the lack of a permanent connection between the cylinders and the engine block housing the crankshaft, enabling variation in compression ratio by axial movement of the cylinder assembly.

The cylinder displacement mechanism consists of multiple components. The integration of these additional parts necessitated several design changes, including modifications to the engine's cooling system. The original coolant discharge system comprised a manifold with three segments connected by rubber hoses (Fig. 1).

The coolant manifold is mounted to the cylinders at the locations indicated in Fig. 2.

Fig. 1. Factory elements of the engine cooling system; manifold draining liquid from the cylinder block
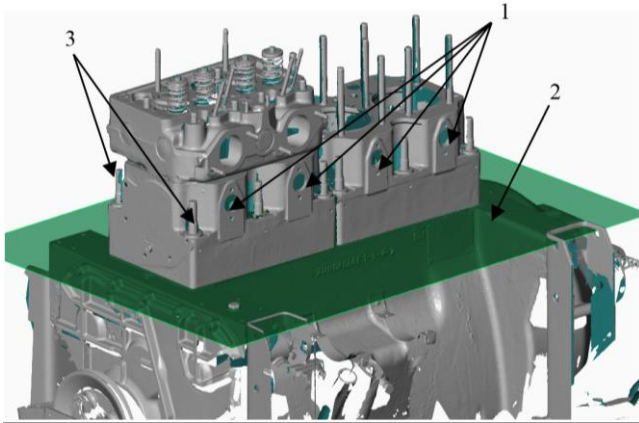

Fig. 2. 3D scan of the base engine: 1 – places for mounting the factory manifold, draining liquid from the cylinder block; 2 – the plane of division of the cylinder block and the engine block; 3 – pins on which the support plate is mounted

One of the key components of the cylinder displacement mechanism is the support plate, which is mounted on additional guide pins (Fig. 2). Unfortunately, the support plate interferes with the factory-installed coolant outlet manifold (Fig. 3). As a result, it was necessary to design new components to resolve this interference. The newly developed parts are flanges, which are mounted to the cylinder block prior to the installation of the support plate (Fig. 5).
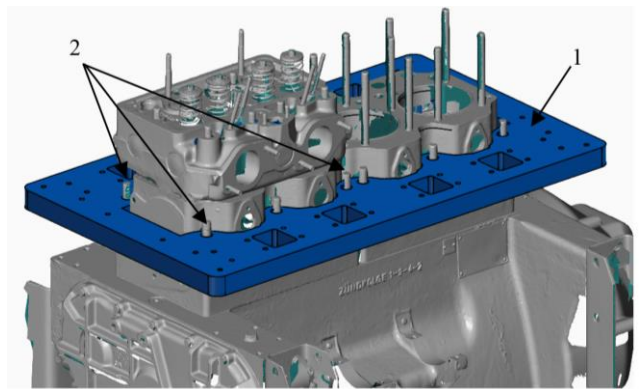

Fig. 3. 3D scan of the base engine with the CAD model of the main support plate of the cylinder block shift mechanism: 1 – support plate; 2 – threaded parts of the plate fixing pins (screwed with nuts)

After the support plate is mounted to the cylinder block, outlet pipes are screwed into the flanges and connected to the hoses. These modifications require additional changes – most importantly, the cross-sectional area of each of the four outlet channels coming from the cylinder block must be reduced. The cross-sectional area has been decreased by a factor of four. Applying the mass balance equation for fluid flow to the modified cross-sectional area yields:

$$\dot{m}_1 = \dot{m}_2 = \rho_1 \cdot v_1 \cdot A_1 = \rho_2 \cdot v_2 \cdot A_2 \tag{1}$$

where (indexes apply to sections 1 and 2): $\dot{m}$ – mass flow rate through cross-section A, ρ – fluid density, v – fluid velocity, A – cross-section area.

Since the coolant can be treated as an incompressible fluid, the density remains constant, i.e., $\rho_1 = \rho_2$. Consequently, a fourfold reduction in cross-sectional area requires a fourfold increase in fluid velocity to maintain the same mass flow rate, according to the principle of continuity. The continuity equation, expressed in Cartesian coordinates, takes the following form:

$$\frac{\partial \rho}{\partial t} + \frac{\partial \rho u}{\partial x} + \frac{\partial \rho v}{\partial y} + \frac{\partial \rho w}{\partial z} = 0 \tag{2}$$

where: ρ – fluid density, t – time, u, v, w – velocity component in, respectively, the x, y and z direction.

Many problems result from the increase in fluid velocity combined with cross-section changes and rapid flow direction changes. First of all, the value of local flow resistance increases and the flow character (laminar or turbulent) varies. Figure 4 shows the engine model with the mechanism for changing the compression ratio. The illustration shows the extent to which the space for the coolant manifold is limited.
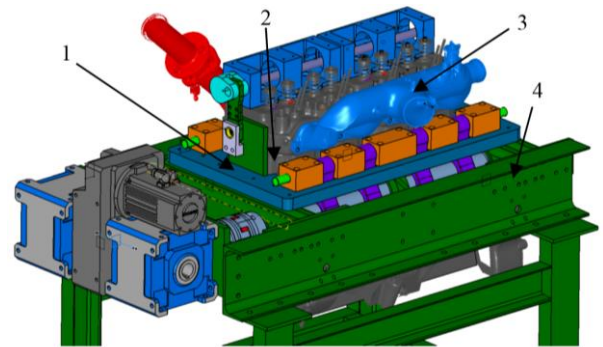

Fig. 4. VCR engine model with mechanism for changing the compression ratio: 1 – support plate; 2 – cylinder block; 3 – intake manifold; 4 – support structure element

The flanges described above with screw-in outlet pipes mounted on the engine are shown in Fig. 5 and 6.
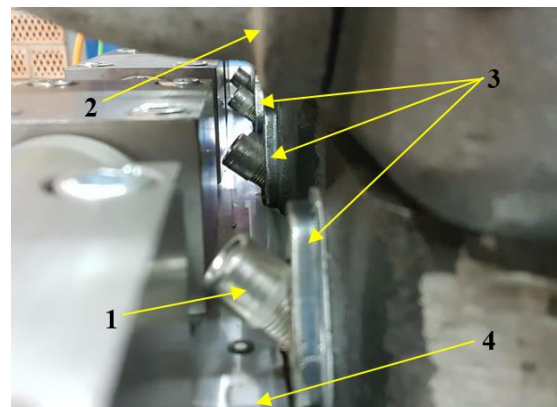

Fig. 5. Modified coolant outlet from the cylinder block (view along the axis of the engine shaft): 1 – outlet pipes; 2 – engine intake manifold; 3 – flanges; 4 – support plate
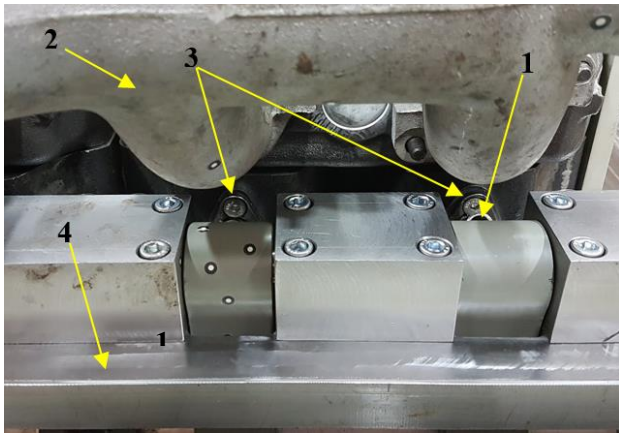
Fig. 6 Modified coolant outlet from the cylinder block (side view): 1 – outlet pipes; 2 – engine intake manifold; 3 – flanges; 4 – support plate

2. Research methodology

Based on the factors described above, outlet coolant manifolds were designed with geometries that accommodate the available space constraints. Figure 7 presents a comparison of the proposed models. These models were created using CATIA V5, exported in a standard CAD data exchange format (STEP), and then imported into the Autodesk CFD environment, where three-dimensional numerical flow analysis was performed.
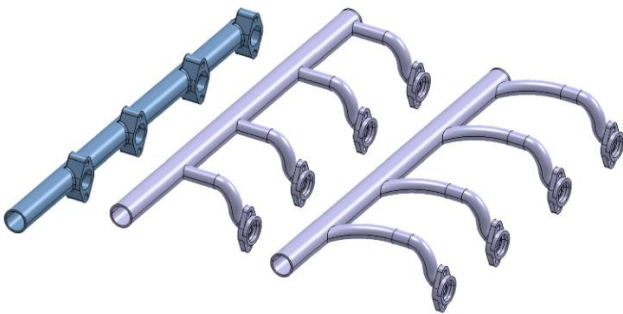

Fig. 7. Comparison of outlet coolant manifold models; from the left: factory manifold (mod0), modified version 1 (mod1), modified version 2 (mod2)

Figure 8 shows a comparison of coolant manifold models in version 1 (mod1) and 2 (mod2) mounted on the engine. A very small space is available for assembling them. It is mostly limited by the engine intake manifold and connecting rods of the cylinder block shifting system (used to change the compression ratio). An electric coolant pump was used in the construction of the prototype engine. The pump mass flow efficiency was calculated according to the formula (3) [9]:

$$\dot{m} = \frac{Q}{c_w \Delta T_w} \qquad (3)$$

where: Q – heat taken from the engine, c_w – specific heat of the coolant, ΔT_w – temperature difference of the coolant flowing out and flowing in the engine.

According to formula (2) for the factory engine, the theoretical cooling mass flow $\dot{m}$ should be 1.9 kg/s (for water). Thus, the mass flow rate for each coolant manifold inlet is 0.48 kg/s. It was assumed that the total coolant stream is divided into four equal parts and its value is constant over

time. For all tested manifolds, a simulation of the flow for two fluids – water and a mixture of ethylene glycol and water (50% by volume) – was carried out. During the analysis, it was assumed that the temperature, density, and dynamic viscosity of the coolant were constant. The simulations were carried out for two values of outlet back pressure (Fig. 8): 0 and 80 kPa [23].

The shape and size of the cross-sections at the manifold inlet were determined by the geometry of the openings in the cylinder block walls, while at the outlet, they were matched to the factory manifold in order to avoid the need for modifications to other components in the cooling system. It was also assumed that the factory flow channels upstream of the inlet and downstream of the outlet would perform their function properly, and their geometry was not considered in the simulation.
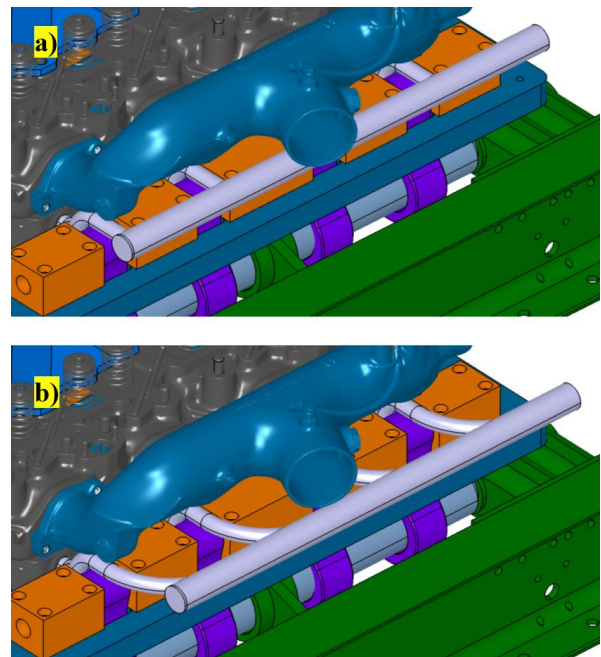

Fig. 8. Modified coolant manifolds on the engine: a) mod1, b) mod2

The symbolic names of individual simulations are presented in Table 1. The physical parameters of water and its mixtures with ethylene glycol at 20°C are given in Table 2.

Figure 9 shows the liquid inlets and outlet in the mod0 version. The back pressure is defined as overpressure relative to the ambient pressure.

The aim of the simulations was to compare the behavior of the coolant stream during flow through the different outlet manifold models. Research results play an auxiliary role in choosing the right design solution. It should be noted that the possibilities of obtaining significantly different versions of coolant manifolds are quite limited due to the very small available space. The work focused mainly on the analysis of trace lines and the distribution of coolant velocity at critical locations of manifold models. It is important to determine the areas or shapes of the channels in manifolds that can disturb the desired fluid flow. The heat transfer analysis was not included in the simulation. Therefore, no calculations for higher temperature values were carried out – this will be the subject of further studies.

Table 1. List of simulation names used in calculations

Outlet coolant manifold	Simulation name	Coolant	Back pressure [kPa]
	mod0-W-p0	Water	0
	mod0-W-p80		80
	mod0-WG-p0	Mixture of ethylene glycol and water (50% by volume)	0
	mod0-WG-p80		80
	mod1-W-p0	Water	0
	mod1-W-p80		80
	mod1-WG-p0	Mixture of ethylene glycol and water (50% by volume)	0
	mod1-WG-p80		80
	mod2-W-p0	Water	0
	mod2-W-p80		80
	mod2-WG-p0	Mixture of ethylene glycol and water (50% by volume)	0
	mod2-WG-p80		80

Table 2. Physical parameters of the analyzed coolants [1]

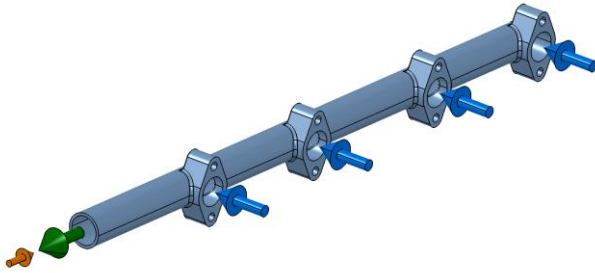| Parameter	Density [g/cm^3]	Dynamic viscosity [mPa·s]
Water	0.9982	1.00
Mixture of ethylene glycol and water (50% by volume)	1.0695	3.98

Fig. 9. Inlets (blue arrows) and outlet (green arrow) on the example of the factory manifold; the orange arrow symbolizes back pressure

3. Results and discussion

Due to the limited volume of the article, it was decided to present selected, representative forms of the results of the coolant flow simulation. Because a wider comparison of modified coolant manifolds (mod1 and mod2) is presented further on, only the results for water flow with 0 kPa back pressure for the factory manifold mod0 are presented here. The color scale for each visualization has been unified, so a given color indicates the same value in each figure. In Figs. 10 to 19, for better readability, the coolant trace lines are shown in individual illustrations.

Figures 12–26 show the results only for mod1 and mod2. The necessary modifications used in the mod1 and mod2 versions resulted in a rapid increase in fluid velocity (Fig. 12–19). Local reduction of the cross-section area also brings an increase in the value of the local resistance coefficient ξ. In the studied cases, the value of this coefficient is about 9.
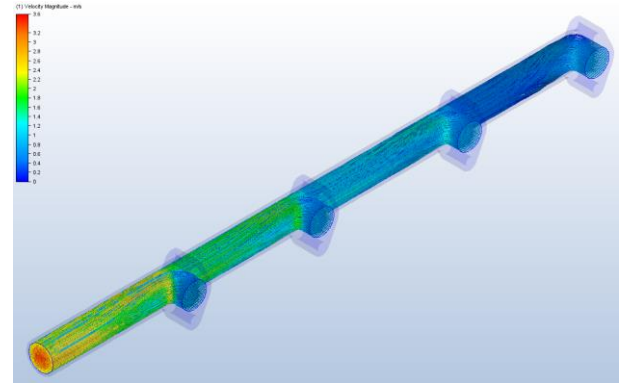
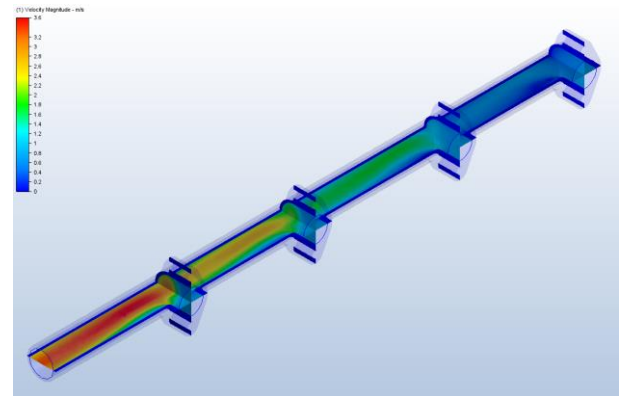Fig. 10. Coolant trace lines with velocity distribution; mod0-W-0kPa

Fig. 11. Distribution of coolant velocity on selected planes; mod0-W-0kPa
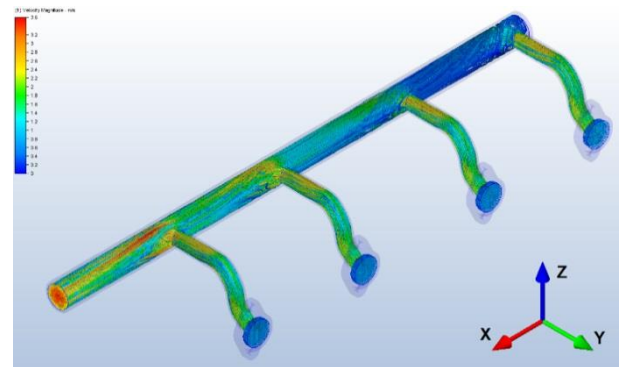
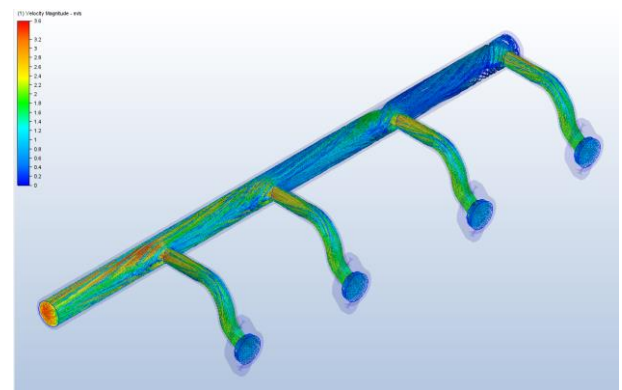Fig. 12. Coolant trace lines with velocity distribution; mod1-W-0kPa

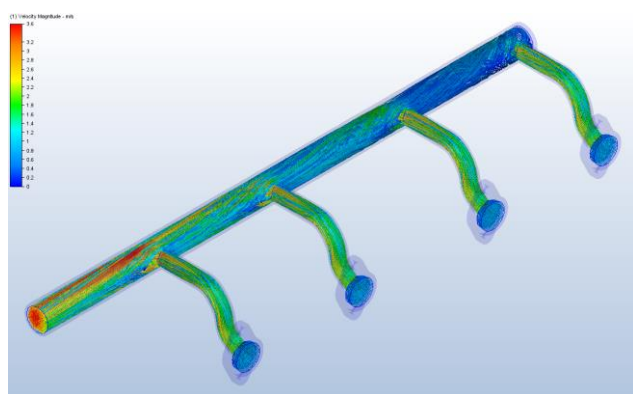Fig. 13. Coolant trace lines with velocity distribution; mod1-WG-0kPa

Fig. 14. Coolant trace lines with velocity distribution; mod1-W-80kPa
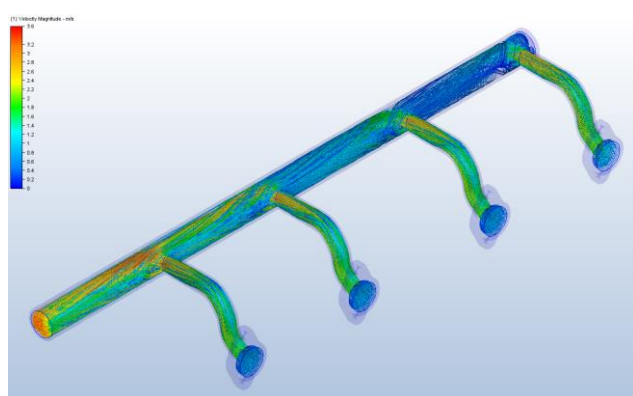

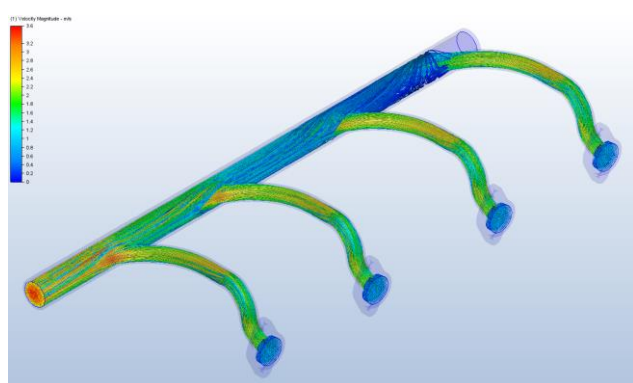Fig. 15. Coolant trace lines with velocity distribution; mod1-WG-80kPa

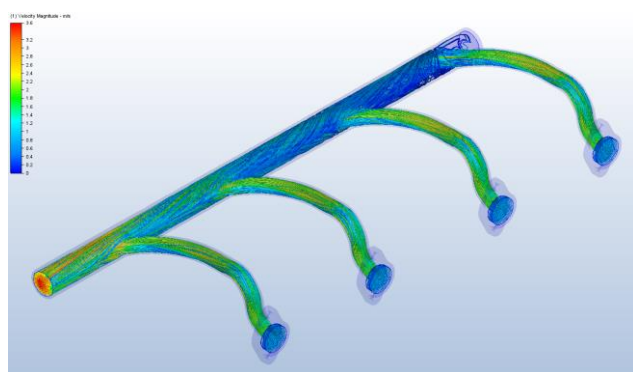Fig.16. Coolant trace lines with velocity distribution; mod2-W-0kPa

Fig. 17. Coolant trace lines with velocity distribution; mod2-WG-0kPa
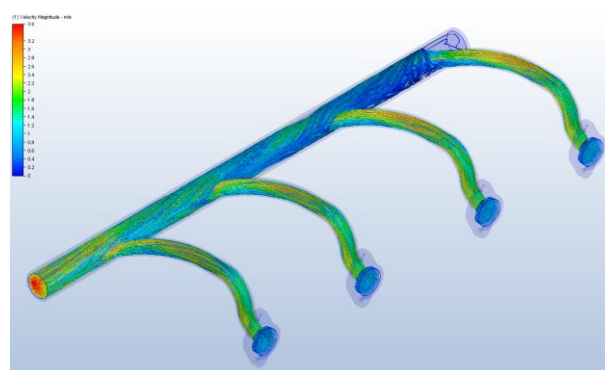

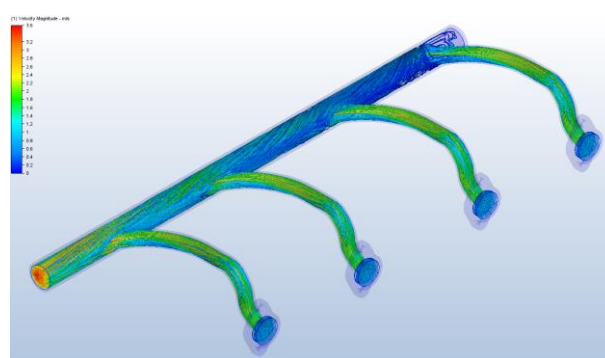Fig. 18. Coolant trace lines with velocity distribution; mod2-W-80kPa

Fig. 19. Coolant trace lines with velocity distribution; mod2-WG-80kPa.

The velocity distribution (Fig. 20) shows that the water flow reaches higher values than that of the water–glycol mixture, and it occurs close to the manifold outlet pipe axis. This dependence is visible for both 0 and 80 kPa back pressure. In addition, in the considered plane (Fig. 20), the water flow at the outlet shows a more uniform velocity profile than that of the mixture of water with ethylene glycol.
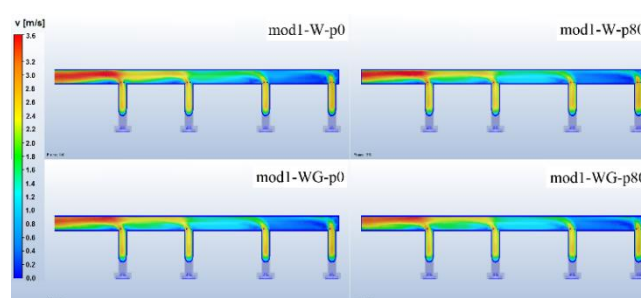

Fig. 20. Distribution of coolant velocity in the mod1 manifold on a plane passing through the axis of the outlet pipe of the manifold and parallel to the XY plane (Fig. 12)

Another undesirable feature of the modified manifolds is the space in which the trace lines are shown in Fig. 21 and 23. This volume is harmful from the point of view of the continuity of the coolant fluid stream. Its existence introduces the risk of local turbulence, which also increases the local flow resistance coefficient. For the mod1 version (Fig. 21), the formation of turbulent flow is slightly dependent on both the type of liquid and the back pressure value.
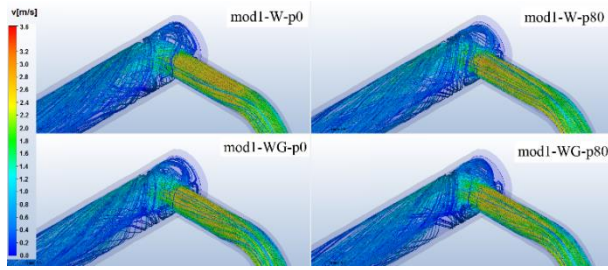
Fig. 21. Comparison of coolant trace lines for mod1

Each inlet channel of the mod1 manifold lies in one plane, which allowed for comparison of velocity distribution in individual sections (Fig. 22).
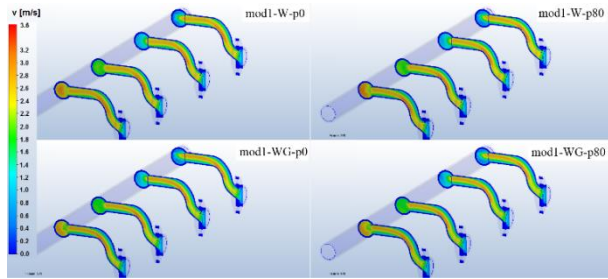

Fig. 22. Coolant velocity distributions in the planes passing through the inlet axes parallel to the YZ plane (Fig. 12); mod1

The considered space for the mod2 manifold causes a visible impact of the type of liquid on the risk of turbulent flow. The results (Fig. 23) show that this risk is greater for a glycol and water mixture than for water alone, both for 0 and 80 kPa back pressure.
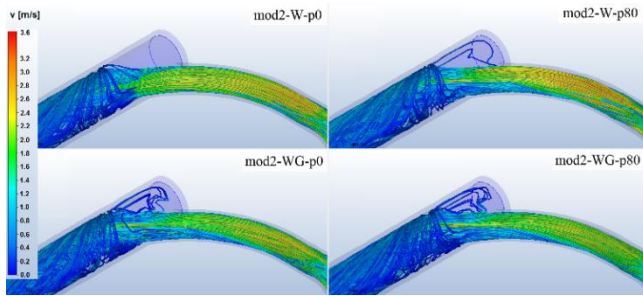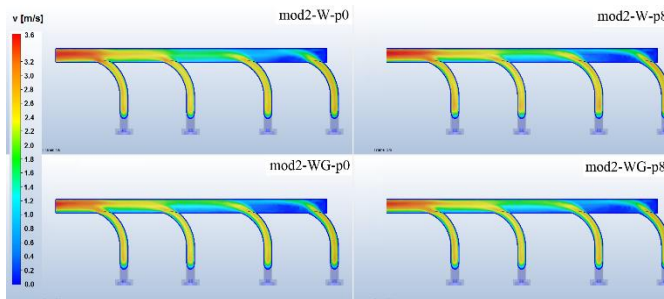

Fig. 23. Comparison of coolant trace lines for mod2

Fig. 24. Distribution of coolant velocity in the mod2 manifold on a plane passing through the axis of the outlet pipe of the manifold and parallel to the XY plane (Fig. 12)

Figures 25 and 26 show that using the mod1 version causes greater differences in velocity in the outlet axis for different simulation conditions than using the mod2 version. The differences reach 15% for water. For a water–glycol mixture, the differences are clearly smaller.
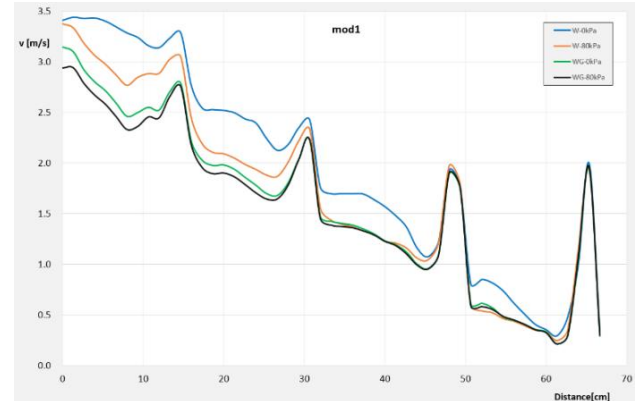
Fig. 25. Coolant velocity for mod1 in the axis shown in Fig. 27

For the mod2 version, the differences in coolant fluid velocity depending on the back pressure are noticeably smaller than for the mod1 version (Fig. 26).
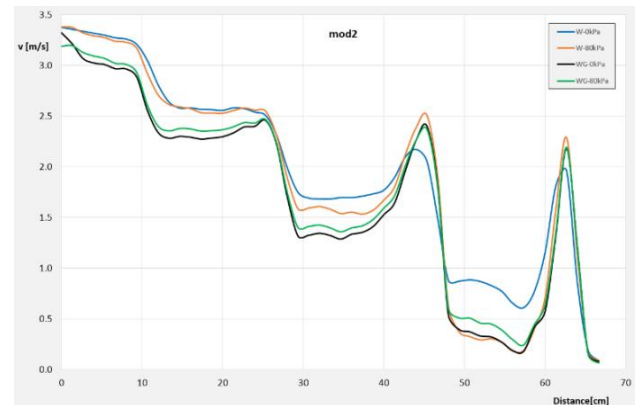
Fig. 26. Coolant velocity for mod2 in the axis shown in Fig. 26

For the mod2 version, the coolant velocity values for the first inlet channels (furthest from the outlet) to the main pipe area have a similar value – about 2.5 m/s. For mod1, the values are significantly different, in the range from 2.0 to 2.5 m/s.
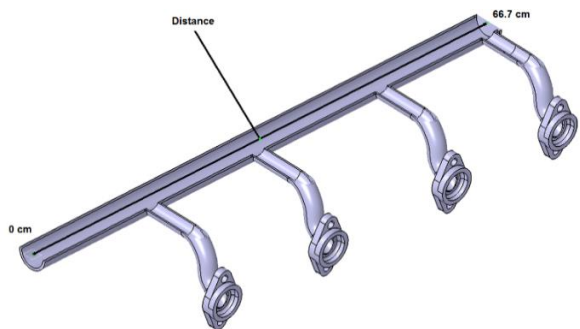
Fig. 27. Explanation of the "Distance" parameter using the example of the mod1 manifold (for charts in Fig. 25 and 26)

Conclusions

An important consideration is the behavior of the coolant streams in regions such as manifold inlet and outlet

connectors, channel curvatures, and spaces that do not contribute to flow but are technologically necessary or difficult to eliminate.

During the design of the engine coolant manifold, it is essential to avoid unintended voids that could disrupt the flow.

The mod2 manifold exhibits a more favorable geometry for coolant flow. Its channel shapes help reduce the risk of turbulence. However, alternative geometrical configurations are also worth exploring.

The simulation was conducted for two different fluids and for manifolds with four inlets and one outlet. As a result, the Reynolds number varies significantly: from 17,900 to 72,900 for water, and from 4200 to 18,400 for a water–glycol mixture. Under actual operating conditions, the flow is considered turbulent across this entire range, due to factors inherent to such systems (e.g., uneven channel surface roughness, vibrations).

It is therefore reasonable to conduct further simulations to evaluate:
- the optimal channel curvature
- the effect of temperature on flow behavior
- heat transfer characteristics based on material selection.

Nomenclature

A	cross-sectional area
CFD	computational fluid dynamics
c_w	specific heat of the coolant
modx	name of the coolant manifold in simulation; x – number of manifold version (0 is for factory manifold); 1, 2 – modified versions
modx-W-p0	name of simulation for modx manifold with water flow and 0 kPa back pressure
modx-W-p80	name of simulation for modx manifold with water flow and 80 kPa back pressure
modx-WG-p0	name of simulation for modx manifold with mixture of ethylene glycol and water (50% by volume) flow and 0 kPa back pressure
modx-WG-p80	name of simulation for modx manifold with mixture of ethylene glycol and water (50% by volume), flow and 80 kPa back pressure
$\dot{m}$	mass flow rate, kg/s
Q	heat removed from the engine
ρ	fluid density
R_e	Reynolds number
ΔT_w	temperature differential between the engine coolant inlet and outlet
v	fluid velocity, m/s
VCR	variable compression ratio

Bibliography

[1] Anton Paar GmbH. Automotive antifreeze. https://wiki.anton-paar.com/en/automotive-antifreeze (accessed on 11.05.2025).

[2] Biały M, Pietrykowski K, Tulwin T, Magryta P. CFD numerical simulation of the indirect cooling system of an internal combustion engine. Combustion Engines. 2017; 170(3):8-18. https://doi.org/10.19206/CE-2017-302

[3] Brusiani F, Falfari S, Forte C, Cazzoli G Verziagi P, Ferrari M et al. Definition of a CFD methodology to evaluate the cylinder temperature distribution in two-stroke air cooled engines. Energy Proced. 2015;81:765-774. https://doi.org/10.1016/j.egypro.2015.12.082

[4] Coclite A, Faruoli M, Viggiano A, Caso P, Magi V. Liquid-cooling system of an aircraft compression ignition engine: A CFD analysis. Fluids. 2020;5(2):71. https://doi.org/10.3390/fluids5020071

[5] Ghare PP, Khalane H, Wakhure U, Khobragade T, Chaudhari S, Jahirabadkar A. Improving heat transfer in single cylinder DI engine through optimization of coolant flow distribution. SAE Technical Papers. 2015-01-1663. 2015. https://doi.org/10.4271/2015-01-1663

[6] Güçlüten GE, Tüccar G. Investigation of the effect of changing air flow velocities in electric vehicles on cylinder geometry battery based on computational fluid dynamics (CFD) analysis. Eur J Sci Technol. 2021;24:240-246. https://doi.org/10.31590/ejosat.899811

[7] Hemmatkhanloo R, Mohammadi A, Varmazyar M. Research on modification of cooling passage for a 4-cylinder turbocharged SI engine with precise cooling viewpoint. J Engine Res. 2016;41(Winter):31-39. https://civilica.com/doc/691372/

[8] Jaskiernik M, Buczek K, Walkowiak J. Simulation of the oil supply through the connecting rod to the piston cooling channels in medium speed engines. Combustion Engines. 2020;180(1):25-30. https://doi.org/10.19206/CE-2020-104

[9] Jędrzejowski J. Obliczanie tłokowego silnika spalinowego (in Polish). WNT. Warszawa 1984.

[10] Johansson A, Gunnarsson J. Predicting flow dynamics of an entire engine cooling system using 3D CFD. Master's thesis. Luleå University of Technology. Luleå 2017.

[11] Li A, Yuen ACY, Wang W, Weng J, Yeoh GH. Numerical investigation on the thermal management of lithium-ion battery system and cooling effect optimization. Appl Therm Eng. 2022;215:118966. https://doi.org/10.1016/j.applthermaleng.2022.118966

[12] Li W, Li E, Shi W, Li W, Xu X. Numerical simulation of cavitation performance in engine cooling water pump based on a corrected cavitation model. Processes. 2020;8(3):278. https://doi.org/10.3390/pr8030278

[13] Murakami Y, Kurosaka H, Kamiya H. Practical application of combustion simulation using CFD for small engine of two-wheeled vehicle. SAE Trans J Engines. 2004;113(3): 1732-1740. https://doi.org/10.4271/2004-32-0006

[14] Pietrykowski K, Tulwin T. Aircraft radial engine CFD cooling model. SAE Int J Engines. 2014;8(1):82-88. https://doi.org/10.4271/2014-01-2884

[15] Pradhan S, Kumari K, Barua A, Panicker RV, Singh H, Jeet S. Numerical simulation of heat transfer and design optimization of IC engine fins geometry using finite element analysis. Int J Interact Des Manuf. 2024;18(1):479-491. https://doi.org/10.1007/s12008-023-01602-3

[16] Shingare AP, Totla NB. Simulation of jacket cooling of a liner of four cylinder diesel engine for genset application. Int Eng Res J (IERJ). 2016:1276-1283. https://www.ijfeat.org/issuepage/august16.php

[17] Souza GR de, Pellegrini CC de, Ferreira SL, Soto Pau F, Armas O. Study of intake manifolds of an internal combustion engine: A new geometry based on experimental results and numerical simulations. Therm Sci Eng Prog. 2019;9: 248-258. https://doi.org/10.1016/j.tsep.2018.12.003

[18] Sroka ZJ, Sufe G, Kejela E. Improving heat transfer in an air-cooled engine by redesigning the fins. Combustion Engines. 2024. https://doi.org/10.19206/CE-195440

[19] Stanivuk T, Lalić B, Mikuličić JŽ, Šundov M. Simulation modelling of marine diesel engine cooling system. Trans Marit Sci. 2021;10(1):112-125. https://doi.org/10.7225/toms.v10.n01.008

[20] Takahashi Y, Yoshitsugu G. CFD air flow analysis for air-cooled motorcycle engines. Honda R&D Technical Review. 2018;18(2):140-147.

[21] Tan L, Yuan Y, Huang C. CFD modelling on flow field characteristics of engine cooling water jacket and its cooling performance improvement based on coolant transport path analysis method. Proc Inst Mech Eng A. 2023;237(2):385-401. https://doi.org/10.1177/09576509221116503

[22] Tang GZ, Zhang L, Jiao ZS. Design and improvement of engine cooling water jacket. Neiranji Gongcheng/Chinese Int Combust Eng Eng. 2014;35(4):91-96.

[23] Wajand JA, Wajand JT. Tłokowe silniki spalinowe (in Polish). WNT. Warszawa 2000.

[24] Zheng QP, Zhang HM, Li S. Flow analysis in cooling water jacket of engine based on three dimensional CFD technology. Neiranji Gongcheng/Chinese Int Combust Eng Eng. 2009;30(6).

Mirosław Jakubowski, DEng. – Department of Automotive Vehicles and Transport Engineering, Rzeszow University of Technology, Poland.
e-mail: *mjakubow@prz.edu.pl*